engineering proceedings

MDPI

Proceeding Paper

Nonlinear Analytical Contact Model for Single-Scale Rough Surfaces †

Guido Violano *, Marco Ceglie, Nicola Menga, Giuseppe Pompeo Demelio and Luciano Afferrante

Department of Mechanics, Mathematics and Management, Polytechnic University of Bari, 70125 Bari, Italy

* Correspondence: guido.violano@poliba.it

† Presented at the 54th Conference of the Italian Scientific Society of Mechanical Engineering Design (AIAS 2025), Florence, Italy, 3–6 September 2025.

Abstract

Classical contact mechanics typically relies on simplifying assumptions such as linear elasticity and frictionless interfaces. A notable example is the Westergaard model, a rigorous theoretical solution for the contact between a rigid sinusoidal surface and an elastic half-space with a flat surface. This configuration captures the features of surface roughness at a single characteristic scale. Such modeling is particularly relevant since most natural and engineered surfaces exhibit roughness, significantly influencing their contact behavior. In this work, we present a nonlinear analytical contact model, which overcomes the main limitations of the Westergaard solution. Specifically, we formulate the contact problem within a finite elasticity framework and include interfacial friction. The analytical model is derived from the results of dedicated finite element simulations and subsequently validated against experimental data from the literature, demonstrating improved predictive accuracy in estimating the contact area as a function of the applied mean pressure. This work lays the foundation for the development of weakly nonlinear multiscale models, where solutions for single-scale roughness can be superimposed to approximate the behavior of more complex, fractal surface geometries. Such an approach holds promise for applications in areas such as tactile human–device interactions, soft robotics, and the design of bioinspired surfaces.

Keywords: nonlinear contact mechanics; finite elasticity; friction

1. Introduction

The study of how bodies and surfaces interact when brought into contact is a central topic in tribology, with applications ranging from mechanical seals and tires to biomedical devices and biological tissues [1]. Classical contact mechanics has long provided a solid foundation for describing these interactions, relying on simplifying assumptions such as linear elasticity, small deformations, and idealized interface conditions [2]. These assumptions have enabled the development of elegant analytical solutions and efficient numerical methods [3,4], offering insight into the influence of surface geometry, material properties, and loading conditions on the contact response.

One notable example within this classical framework is the model proposed by Westergaard [5], which analytically describes the frictionless contact between a rigid sinusoidal indenter and a linear elastic half-space. This simplified geometry, representing a periodic surface waviness, has been widely used to model surface roughness at a single scale and serves as a basic benchmark for understanding rough contact problems. While such linear

Check for updates

Academic Editors: Nicola Bonora, Umberto Galietti, Luigi Bruno, Davide Castagnetti, Cristiana Del Prete, Mario Guagliano and Vigilio Fontanari

Published: 31 March 2026

Copyright: © 2026 by the authors. Licensee MDPI, Basel, Switzerland. This article is an open access article distributed under the terms and conditions of the Creative Commons Attribution (CC BY) license.

solutions remain useful in many contexts, they fall short in capturing the complex behavior observed in materials and interfaces subjected to large strains or significant frictional effects [6,7].

In practice, surfaces often display roughness over multiple length scales [8,9], and the materials involved, particularly soft solids like polymers or elastomers, can undergo large, nonlinear deformations. In such cases, the assumptions of classical theory no longer apply. Recent experimental and computational studies have revealed phenomena such as nontrivial stress distributions, contact hysteresis, and frictional energy dissipation, which cannot be explained by linear models alone [7,10,11]. These effects are particularly evident in systems where the geometry or material properties introduce coupling between normal and tangential directions [12], even in the absence of adhesion or viscoelasticity.

Moreover, even the simple estimation of the contact area becomes complicated when material and geometric nonlinearities, as well as friction, come into play [6,13]. Material nonlinearities occur when the stress–strain relationship deviates from linear elasticity, meaning the stiffness is no longer constant. This includes hyperelastic materials, or materials whose response evolves with the applied load. Geometric nonlinearities arise when deformations are large enough to significantly change the surface configuration, thereby altering the contact distribution itself. The presence of friction further complicates the picture, as tangential forces interact with normal components, dynamically influencing the evolution of the contact area during loading.

This work aims to extend the analytical modeling of rough contact by relaxing the key assumptions of classical solutions [5]. We develop a new analytical model for the contact between a rigid wavy profile and a nonlinear elastic solid, incorporating both finite deformations and interfacial friction. The formulation is guided and supported by finite element simulations tailored to this problem, which help identify the critical nonlinear contributions. The model is then compared to available experimental data from the literature, confirming its ability to predict the evolution of contact area under normal loading.

Looking ahead, this study sets the groundwork for future developments in multiscale contact modeling [4,14]. By combining solutions corresponding to single-scale roughness, it will be possible to construct weakly nonlinear multiscale models capable of describing more realistic surface interactions. Such models could offer a powerful balance between analytical tractability and physical fidelity, with broad applicability in engineering and material science.

2. Problem Definition

We consider the two-dimensional frictional contact between a deformable solid and a rigid sinusoidal indenter with amplitude Δ and wavelength λ, as illustrated in Figure 1. The deformable layer is bonded to a rigid slab on its upper surface. A uniform pressure $\bar{p}$ is applied on the upper edge, resulting in a contact region of semi-width a.

The deformable solid is assumed to be nearly incompressible ($\nu \approx 0.5$) and is modeled as Neo-Hookean hyperelastic material, with strain energy density function

$$W = \frac{G}{2}(\bar{I}_1 - 3) + \frac{\kappa}{2}(J-1)^2, \tag{1}$$

where G and κ denote the shear and bulk moduli, J is the determinant of the deformation gradient, and $\bar{I}_1$ is the first invariant of the isochoric right Cauchy-Green tensor [15].

https://doi.org/10.3390/engproc2026131025

Contact interactions are assumed to be adhesionless, while friction is represented using a regularized Coulomb–Orowan law [16], which limits the interfacial shear stress by a threshold

$$\tau_{sl} = \min(\mu p, \tau_{max}), \tag{2}$$

where μ is the friction coefficient, p is the local contact pressure, and τ_{max} is a material-dependent shear strength. This formulation is particularly suitable for polymer–glass interfaces [17].

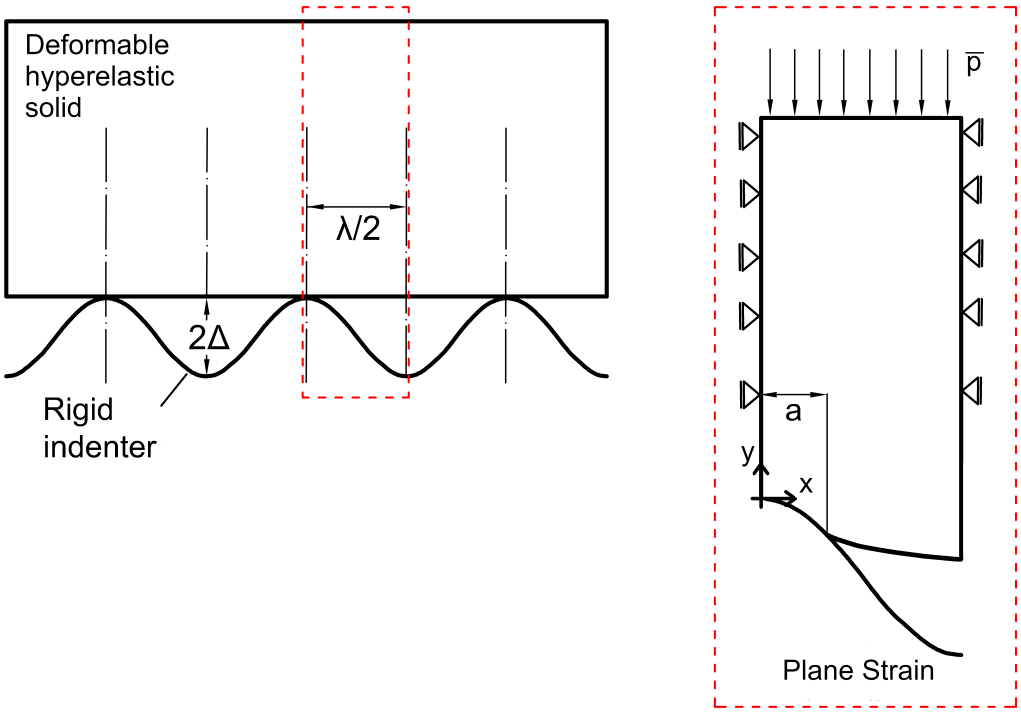


Figure 1. The problem under investigation: a rigid wavy profile is squeezed against a hyperelastic solid.

2.1. Finite Element Model

The finite element model used in this study was originally developed in Ref. [6]. Numerical simulations are carried out using the commercial finite element software ABAQUS/Standard 2019. Exploiting the symmetry and periodicity of the geometry, the computational domain is restricted to half of a sinusoidal wavelength and a plane strain configuration is adopted (see Figure 1). Horizontal displacements are constrained at the lateral boundaries, while a uniform pressure $\bar{p}$ is applied to the top surface of the rigid slab bonded to the deformable solid.

The solid is discretized using hybrid, reduced-integration plane strain elements, which are well suited for nearly incompressible materials. A fine mesh is used near the contact interface to capture steep stress gradients, while a coarser mesh is employed elsewhere to improve computational efficiency. The rigid indenter is modeled as an analytical surface, enabling accurate enforcement of boundary conditions through a reference node.

The simulations are performed within a finite displacement framework to account for large deformations and rotations. All kinematic and stress fields are evaluated in the current (deformed) configuration. The mean pressure $\bar{p}$ is computed by integrating the vertical component of the contact stresses over the deformed interface. For further details on the finite displacement formulation, the reader is referred to Ref. [6].

Normal contact is enforced using a hard pressure-overclosure relationship, while tangential interactions are governed by a penalty-based Coulomb–Orowan friction law. This regularized model avoids convergence issues near the contact edges.

To enhance numerical stability in the presence of material and geometric nonlinearities, a small amount of artificial damping is introduced. The damping parameters are calibrated to ensure negligible impact on the computed internal energy.

All simulations are conducted under force-controlled conditions, with the applied pressure $\bar{p}$ incrementally increased to a target value. Parametric studies are carried out to explore the effects of interfacial friction, material nonlinearity, and indenter geometry on the contact response.

2.2. Westergaard Solution for Frictionless Contact

For comparison, we recall the classical Westergaard solution [5] for the mean contact pressure $\bar{p}$ between a linear elastic half-plane and a rigid sinusoidal indenter with amplitude Δ and wavelength λ under frictionless conditions:

$$\bar{p}(a) = \frac{E^* \pi \Delta}{\lambda} \sin^2\left(\frac{a\pi}{\lambda}\right), \tag{3}$$

where $E^* = \frac{E}{1-\nu^2}$ is the plane strain modulus, E is Young's modulus, ν the Poisson's ratio, and a is the contact half-width.

3. Nonlinear Analytical Model

To capture deviations from the linear elastic Westergaard solution caused by friction and nonlinearities, we propose a nonlinear analytical model that introduces empirical correction functions to the mean contact pressure. The corrected mean pressure $\bar{p}_{nl}$ is expressed as

$$\bar{p}_{nl}(\lambda, \Delta, \tau_{\max}, a) = \bar{p}(a)\left[B(AR, \tau_{\max}) + a\, A(AR, \tau_{\max}) \cos^2\left(\frac{a\pi}{\lambda}\right)\right], \tag{4}$$

where $\bar{p}(a)$ is the Westergaard mean pressure from Equation (3), $AR = \Delta/\lambda$ is the dimensionless aspect ratio, and $\tau_{\max}$ is the maximum interfacial shear stress. The correction functions A and B depend on AR and $\tau_{\max}$, and are fitted using polynomial models:

$$A(AR, \tau_{\max}) = a_0 + a_1 AR + a_2 \tau_{\max} + a_3 AR^2 + a_4 AR\tau_{\max} + a_5 \tau_{\max}^2, \tag{5}$$

$$B(AR, \tau_{\max}) = b_0 + b_1 AR + b_2 \tau_{\max} + b_3 AR^2 + b_4 AR\tau_{\max} + b_5 \tau_{\max}^2. \tag{6}$$

The coefficients $\{a_i\}$ and $\{b_i\}$ are obtained from nonlinear regression on numerical data sets spanning a range of typical values of AR and $\tau_{\max}$ (see Figure 2) and are summarized in Table 1.

Table 1. Fitted coefficients for the polynomial correction functions $A(AR, \tau_{\max})$ and $B(AR, \tau_{\max})$.

Coefficient	A	B
$a_0 - b_0$	0.24536	0.963506
$a_1 - b_1$	−9.96905	1.26005
$a_2 - b_2$	4.80482	−0.33278
$a_3 - b_3$	−0.305098	−0.424387
$a_4 - b_4$	−47.5605	10.4263
$a_5 - b_5$	−3.56199	−2.45931

https://doi.org/10.3390/engproc2026131025

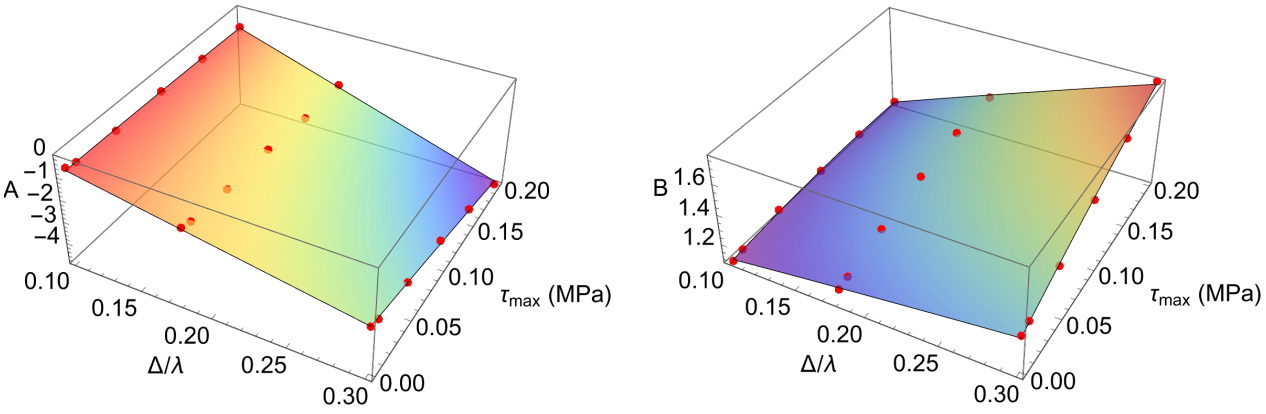


Figure 2. Empirical correction functions $A(AR, \tau_{\max})$ and $B(AR, \tau_{\max})$ fitted via polynomial regression, showing their dependence on the dimensionless aspect ratio $AR = \Delta/\lambda$ and the maximum shear stress $\tau_{\max}$.

4. Results

4.1. Comparison with FE Predictions

To test the robustness of the correction functions introduced in the nonlinear analytical model, here referred to as the Westergaard NonLinear (WNL) model, we compare its predictions against finite element simulations and the classical Westergaard solution [5]. The comparison is conducted over a broad set of conditions, including aspect ratios $AR = \Delta/\lambda$ equal to 0.1, 0.18, and 0.3, and interfacial shear strength values $\tau_{\max} = 0, 0.01, 0.05, 0.1, 0.15,$ and 0.2 MPa. These values are representative of real surface roughness [18] and frictional interfaces typically encountered in soft materials and biological systems [19].

Figure 3 reports the dimensionless mean contact pressure $\bar{p}/E^*$ as a function of the normalized contact half-width a/λ. Each plot displays the finite element results (gray circles), the WNL model prediction (solid red line), and the classical Westergaard solution (solid black line).

The WNL model shows excellent agreement with the FEM data across the entire range of parameters considered. Notably, even in the case $\tau_{\max} = 0$, the FEM results, and also the WNL model, depart from the classical Westergaard prediction at high pressure. This deviation stems from the inclusion of material and geometric nonlinearities, which are not captured by the linear theory. In particular, the use of a hyperelastic constitutive law and the adoption of a finite deformation framework in the numerical and analytical models lead to significant corrections, even in the absence of friction.

At increasing values of $\tau_{\max}$, the WNL model continues to match the FEM results with high fidelity, accurately capturing the nonlinear evolution of contact pressure. The embedded correction functions $A(AR, \tau_{\max})$ and $B(AR, \tau_{\max})$ enable the model to reflect both the trend and magnitude of the pressure–contact width relationship over a wide parameter space.

For each case, the mean squared error (MSE) between the WNL model and FEM predictions is also reported in the plots. The error remains consistently low across all simulations, typically well below 10^{-3}, confirming the accuracy and consistency of the proposed formulation.

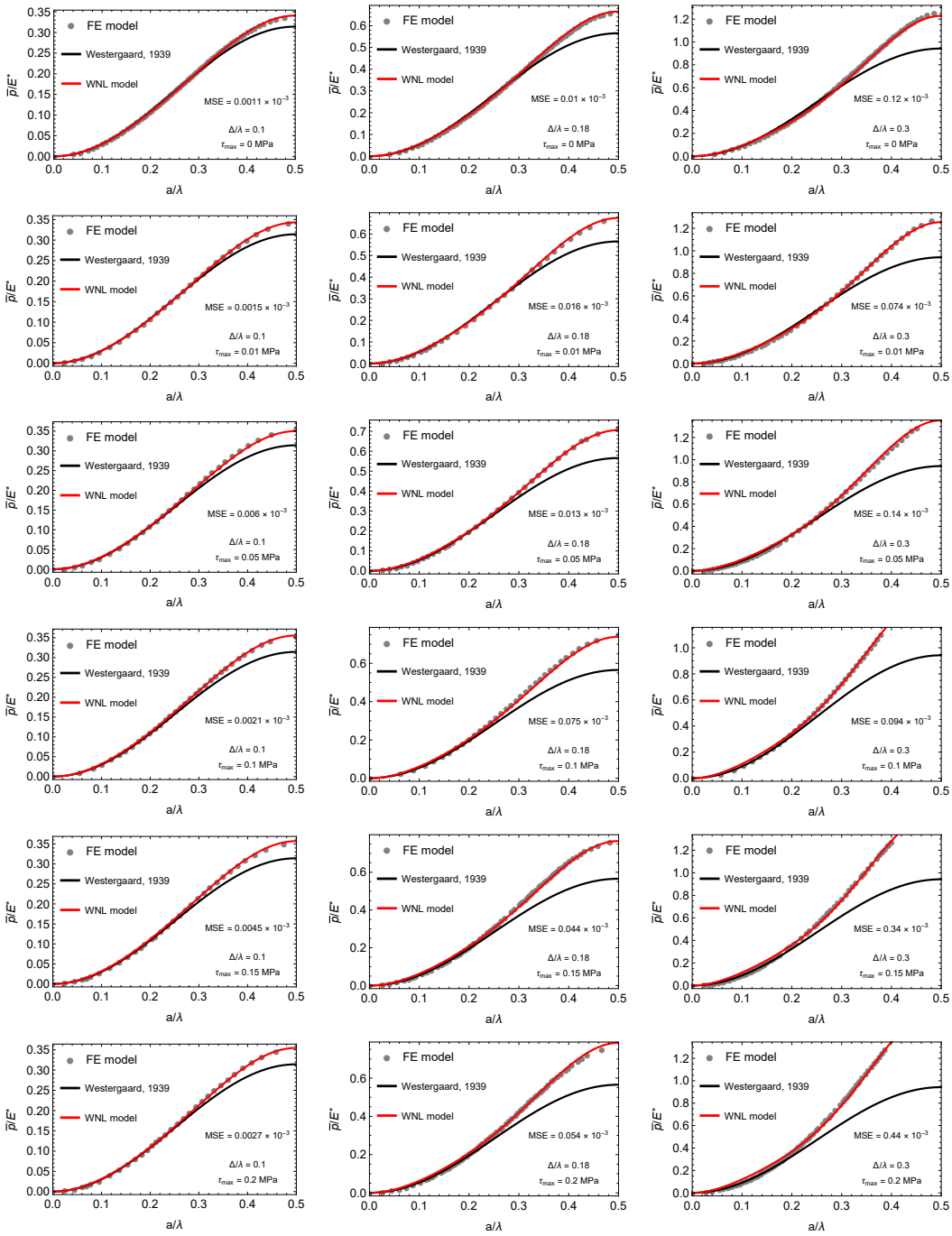


Figure 3. Comparison among FEM simulations (gray circles), the WNL model (solid red line), and the classical Westergaard solution [5] (solid black line) for normalized mean pressure $\bar{p}/E^*$ versus a/λ, across various AR and $\tau_{\max}$ values. MSE values quantify the agreement between FEM and WNL results.

4.2. Comparison with the Experimental Data by Warman and Ennos

The fingertip represents a natural testbed for our contact model due to its distinctive surface topography, as human and primate fingerpads exhibit nearly periodic ridged structures (fingerprints) [20,21], which can be reasonably approximated by sinusoidal profiles (see Figure 4). Previous studies report a typical wavelength $\lambda \approx 0.5\,\text{mm}$ and amplitude $\Delta \approx 0.04\,\text{mm}$ for fingerprint ridges [20]. This geometric regularity aligns well with the assumptions of the proposed model, making it a suitable system for experimental validation.



Figure 4. The ridges of a human fingerprint.

To evaluate the model's predictive capabilities, we compare it against experimental results from Warman and Ennos [22], who performed compression tests on different fingers and measured the evolution of the contact area as a function of the applied normal load. In Figure 5, black squares represent the measured contact area (in mm^2) plotted against the applied load (in N).

In Ref. [22], it is noted that the nominal contact area is approximately 1.4 larger than the measured ridge contact area, consistent with the fingerprint topography. To compare the model predictions with the experimental data, we compute the total contact area based on the model output. The WNL model provides an estimate of the contact half-width a for given input parameters, which allows us to evaluate the contact area per unit length (along the direction orthogonal to the ridges) as $A_{\text{model}} = 2a$.

Assuming that the contact occurs over a circular region with total area $A_{\text{exp}} \approx 200\,\text{mm}^2$, we estimate the equivalent radius as:

$$R = \sqrt{\frac{A_{\text{exp}}}{\pi}} \approx 8\,\text{mm}.$$

Thus, the effective contact length is approximately $2R$, and the total contact area is obtained by:

$$A_{\text{total}} = A_{\text{model}} \cdot N \cdot 2R = 2a \cdot N \cdot 2R,$$

where N is the number of ridges (or wavelengths) present along the contact width. Since the fingerprint wavelength is $\lambda = 0.5\,\text{mm}$, and the total projected width is $2R$, the number of wavelengths is:

$$N = \frac{2R}{\lambda} \approx \frac{16}{0.5} = 32.$$

This procedure allows us to convert the model prediction from a 2D ridge-based area to a total surface area that can be compared with experimental measurements.

Regarding material parameters, human fingerpads exhibit a range of Young's moduli from $E^* = 0.07$ to $0.5\,\text{MPa}$, depending on age, hydration, and anatomical differences [23,24]. For this comparison, we adopt $E^* = 0.15\,\text{MPa}$ as a representative value. As for interfacial friction, Adams et al. [20] report a shear threshold of approximately $\tau_{\text{max}} = 0.05\,\text{MPa}$ for finger–glass contact, which is also adopted here.

Under these assumptions, the WNL model shows excellent agreement with the experimental data (see Figure 5). While some variability in the experimental measurements is expected, due to inter-individual differences, variations in skin elasticity, loading orientation, humidity, and temperature [24,25], this comparison highlights the potential of the WNL model in capturing complex biological contact phenomena with minimal empirical tuning.

Finally, we note that within a nonlinear contact framework the choice of assigning the sinusoidal profile to either the rigid indenter or the deformable half-space is not

strictly equivalent, and may lead to differences in the resulting pressure–area relationship, particularly at high loads. However, within the range of loads considered in the present comparison, such differences are expected to be negligible [7].

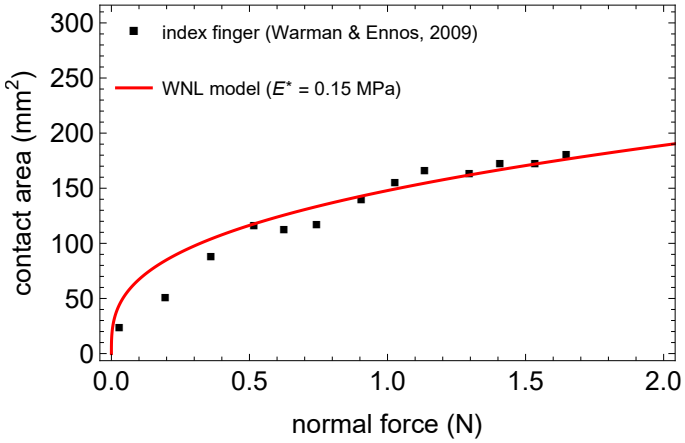


Figure 5. Comparison between the WNL model predictions and the experimental load–area data from Warman and Ennos [22].

5. Conclusions

In this work, we have proposed a novel nonlinear analytical model (WNL model) to describe the normal contact behavior between a rigid sinusoidal indenter and a deformable body, incorporating both material and geometrical nonlinearities as well as interfacial friction effects. The model is based on the classical Westergaard solution [5], which is corrected by means of empirically fitted functions that account for deviations arising from finite deformations and frictional tractions.

Compared to existing analytical solutions that are limited to linear elastic and frictionless contact, the present model offers a significant advancement in predictive capability. By incorporating the effects of finite strain, material nonlinearity, and interfacial shear, it extends the range of applicability of classical theories to more realistic contact conditions, such as those encountered in soft interfaces and biological systems.

The model has been validated through extensive comparison with finite element simulations, showing excellent agreement across a wide range of amplitudes, wavelengths, and frictional parameters. Furthermore, the WNL model has been benchmarked against experimental data available in the literature, particularly from indentation tests on fingers.

Looking forward, this analytical framework lays the groundwork for future multiscale modeling of contact problems involving rough surfaces with hierarchical or fractal-like features [8] and materials with more complicated constitutive behavior [26]. An important extension of this work will be the generalization of the proposed correction scheme to statistically self-affine profiles, enabling the modeling of complex real-world rough interfaces while retaining the computational efficiency of an analytical formulation. Moreover, this work paves the way for future advancements in haptic interfaces, soft robotics, and bioinspired surface design.

Author Contributions: Conceptualization, All the authors; methodology, All the authors; software, G.V. and M.C.; validation, G.V.; formal analysis, G.V. and M.C.; investigation, G.V. and M.C.; data curation, G.V. and M.C.; writing—original draft preparation, G.V.; writing—review and editing, All the authors; supervision, G.V., G.P.D. and L.A.; project administration, G.V. and N.M.; funding acquisition, G.V. and N.M. All authors have read and agreed to the published version of the manuscript.

Funding: This work was supported by the Italian Ministry of University and Research under the Programme "Department of Excellence" Legge 232/2016 (Grant No. CUP-D93C23000100001) and

by the European Union-NextGenerationEU through the Italian Ministry of University and Research under the programs: National Sustainable Mobility Center CN00000023, Italian Ministry of University and Research Decree n. 1033-17/06/2022, Spoke 11—Innovative Materials & Lightweighting; PRIN2022 (Projects of Relevant National Interest) grant nr. 2022SJ8HTC—ELectroactive gripper For mIcro-object maNipulation (ELFIN); PRIN2022 PNRR (Projects of Relevant National Interest) grant nr. P2022MAZHX—TRibological modellIng for sustainaBle design Of induStrial friCtiOnal inteRfacEs (TRIBOSCORE). The opinions expressed are those of the authors only and should not be considered as representative of the European Union or the European Commission's official position. Neither the European Union nor the European Commission can be held responsible for them.

Institutional Review Board Statement: Not applicable.

Informed Consent Statement: Not applicable.

Data Availability Statement: The raw data supporting the conclusions of this article will be made available by the authors on request.

Conflicts of Interest: The authors declare no conflicts of interest.

References

1. Vakis, A.I.; Yastrebov, V.A.; Scheibert, J.; Nicola, L.; Dini, D.; Minfray, C.; Almqvist, A.; Paggi, M.; Lee, S.; Limbert, G.; et al. Modeling and simulation in tribology across scales: An overview. *Tribol. Int.* **2018**, *125*, 169–199. [CrossRef]
2. Johnson, K.L. *Contact Mechanics*; Cambridge University Press: Cambridge, UK , 1987.
3. Müser, M.H.; Dapp, W.B.; Bugnicourt, R.; Sainsot, P.; Lesaffre, N.; Lubrecht, T.A.; Persson, B.N.; Harris, K.; Bennett, A.; Schulze, K.; et al. Meeting the contact-mechanics challenge. *Tribol. Lett.* **2017**, *65*, 118. [CrossRef]
4. Persson, B.N. Theory of rubber friction and contact mechanics. *J. Chem. Phys.* **2001**, *115*, 3840–3861. [CrossRef]
5. Westergaard, H.M. Bearing pressures and cracks: Bearing pressures through a slightly waved surface or through a nearly flat part of a cylinder, and related problems of cracks. *J. Appl. Mech.* **1939**, *6*, A49–A53. [CrossRef]
6. Ceglie, M.; Violano, G.; Afferrante, L.; Menga, N. Finite deformations induce friction hysteresis in normal wavy contacts. *Int. J. Mech. Sci.* **2025**, *291*, 110115. [CrossRef]
7. Ceglie, M.; Violano, G.; Portaluri, L.; Algieri, L.; Afferrante, L.; Scaraggi, M.; Menga, N. Contact Area Shrinkage and Increase in Wavy Frictional Sliding Contacts. *J. Mech. Phys. Solids* **2026**, *206*, 106389. [CrossRef]
8. Persson, B.N. Contact mechanics for randomly rough surfaces. *Surf. Sci. Rep.* **2006**, *61*, 201–227. [CrossRef]
9. Pradhan, A.; Müser, M.; Miller, N.; Abdelnabe, J.; Afferrante, L.; Albertini, D.; Aldave, D.; Algieri, L.; Ali, N.; Almqvist, A.; et al. The surface-topography challenge: A multi-laboratory benchmark study to advance the characterization of topography. *Tribol. Lett.* **2025**, *73*, 110. [CrossRef]
10. Lengiewicz, J.; de Souza, M.; Lahmar, M.A.; Courbon, C.; Dalmas, D.; Stupkiewicz, S.; Scheibert, J. Finite deformations govern the anisotropic shear-induced area reduction of soft elastic contacts. *J. Mech. Phys. Solids* **2020**, *143*, 104056. [CrossRef]
11. Wang, C.; Li, Y.; Li, Y.; Fan, Y.; Feng, Z. Coupling effect of large deformation and surface roughness on dynamic frictional contact behaviors of hyperelastic material. *Comput. Mech.* **2024**, *75*, 455–473. [CrossRef]
12. Müller, C.; Müser, M.H.; Carbone, G.; Menga, N. Significance of elastic coupling for stresses and leakage in frictional contacts. *Phys. Rev. Lett.* **2023**, *131*, 156201. [CrossRef]
13. Mu, T.; Li, R.; Linghu, C.; Liu, Y.; Leng, J.; Gao, H.; Hsia, K.J. Nonlinear Contact Mechanics of Soft Elastic Spheres Under Extreme Compression. *J. Mech. Phys. Solids* **2025**, *203*, 106229. [CrossRef]
14. Violano, G.; Afferrante, L. On the contact between elasto-plastic media with self-affine fractal roughness. *Int. J. Mech. Sci.* **2023**, *255*, 108461. [CrossRef]
15. Kossa, A.; Valentine, M.T.; McMeeking, R.M. Analysis of the compressible, isotropic, neo-Hookean hyperelastic model. *Meccanica* **2023**, *58*, 217–232. [CrossRef]
16. Orowan, E. The Calculation of Roll Pressure in Hot and Cold Flat Rolling. *Proc. Inst. Mech. Eng.* **1943**, *150*, 140–167. [CrossRef]
17. Chateauminois, A.; Fretigny, C. Local friction at a sliding interface between an elastomer and a rigid spherical probe. *Eur. Phys. J. E* **2008**, *27*, 221–227. [CrossRef] [PubMed]
18. Lorenz, B.; Persson, B.; Fortunato, G.; Giustiniano, M.; Baldoni, F. Rubber friction for tire tread compound on road surfaces. *J. Phys. Condens. Matter* **2013**, *25*, 095007. [CrossRef]
19. Nguyen, D.T.; Paolino, P.; Audry, M.; Chateauminois, A.; Fretigny, C.; Le Chenadec, Y.; Portigliatti, M.; Barthel, E. Surface pressure and shear stress fields within a frictional contact on rubber. *J. Adhes.* **2011**, *87*, 235–250. [CrossRef]

20. Adams, M.J.; Johnson, S.A.; Lefèvre, P.; Lévesque, V.; Hayward, V.; André, T.; Thonnard, J.L. Finger pad friction and its role in grip and touch. *J. R. Soc. Interface* **2013**, *10*, 20120467. [CrossRef] [PubMed]
21. Dzidek, B.M.; Adams, M.J.; Andrews, J.W.; Zhang, Z.; Johnson, S.A. Contact mechanics of the human finger pad under compressive loads. *J. R. Soc. Interface* **2017**, *14*, 20160935. [CrossRef]
22. Warman, P.H.; Ennos, A.R. Fingerprints are unlikely to increase the friction of primate fingerpads. *J. Exp. Biol.* **2009**, *212*, 2016–2022. [CrossRef] [PubMed]
23. Oprişan, C.; Cârlescu, V.; Barnea, A.; Prisacaru, G.; Olaru, D.; Plesu, G. Experimental determination of the Young's modulus for the fingers with application in prehension systems for small cylindrical objects. *Proc. IOP Conf. Ser. Mater. Sci. Eng.* **2016** , *147*, 012058. [CrossRef]
24. Abdouni, A.; Djaghloul, M.; Thieulin, C.; Vargiolu, R.; Pailler-Mattei, C.; Zahouani, H. Biophysical properties of the human finger for touch comprehension: Influences of ageing and gender. *R. Soc. Open Sci.* **2017**, *4*, 170321. [CrossRef]
25. Infante, V.H.; Fehlberg, M.; Saikumar, S.; Drewing, K.; Meinke, M.C.; Bennewitz, R. The role of skin hydration, skin deformability, and age in tactile friction and perception of materials. *Sci. Rep.* **2025**, *15*, 9935. [CrossRef]
26. Ogden, R. Large deformation isotropic elasticity—On the correlation of theory and experiment for incompressible rubberlike solids. *Rubber Chem. Technol.* **1973**, *46*, 398–416. [CrossRef]

Disclaimer/Publisher's Note: The statements, opinions and data contained in all publications are solely those of the individual author(s) and contributor(s) and not of MDPI and/or the editor(s). MDPI and/or the editor(s) disclaim responsibility for any injury to people or property resulting from any ideas, methods, instructions or products referred to in the content.